IEEE Access
Multidisciplinary ⋮ Rapid Review ⋮ Open Access Journal

Received 26 March 2023, accepted 4 April 2023, date of publication 6 April 2023, date of current version 12 April 2023.

Digital Object Identifier 10.1109/ACCESS.2023.3265083

RESEARCH ARTICLE

Study of Long-Term Energy Storage System Capacity Configuration Based on Improved Grey Forecasting Model

JIFANG LI[1], SHUO FENG[1], TAO ZHANG[2], LIDONG MA[1], XIAOYANG SHI[1], AND XINGYAO ZHOU[1]

[1]School of Electric Power, North China University of Water Resources and Electric Power, Zhengzhou 450000, China
[2]State Grid Henan Electric Power Company Luoyang Power Supply Company, Luoyang 471009, China

Corresponding author: Shuo Feng (2574958287@qq.com)

This work was supported by the National Natural Science Foundation of China under Grant U1804149.

ABSTRACT Distributed generation equipment improves renewable energy utilization and economic benefits through an energy storage system (ESS). However, dominated by short-term data, the configuration of long-period ESS capacity is absent based on the dynamic change of load, which leads to a large deviation from the expected return. Considering the system characteristics of lack of data and less information, after introducing the grey theory, we propose a new long-term capacity configuration method for ESS and establish the long-term grey forecasting model (GFM) of user load, improving the basic forecasting model to improve the accuracy of the long-term forecasting model. Then, the scheduling model is established with the maximum economic and social benefits as the optimization objective. Based on the forecast data of the improved grey forecasting model (IGFM), the hierarchical solution method is used to solve the scheduling model. Finally, the parameters are configured based on the service life of the equipment and the expected rate of return. The simulation results show that higher accuracy is realized in the improved prediction model, and the improved algorithm gets higher convergence speed and precision. Apart from that, the nonlinear correlation trend of the EES return rate between the capacity and life cycle is revealed. Compared with the ESS configuration in a short period, this study provides more comprehensive and accurate data support for the capacity configuration of the ESS, reducing the error between the actual return and the expected return significantly.

INDEX TERMS Capacity configuration, energy storage system, grey theory, hierarchical optimization, scheduling.

NOMENCLATURE

A. ABBREVIATIONS

ESS	Energy storage system.
GFM	Grey forecasting model.
IGFM	Improved grey forecasting model.
AEO	Artificial ecosystem optimization.
GM (1,1)	First-order univariate gray predictive model.
GM (1, N)	First-order multivariable grey forecasting model.
PSO	Particle swarm optimization.
IPSO	Improved particle swarm optimization.
MOPSO	Multi-objective particle swarm optimization algorithm.
GWO	Grey wolf optimization algorithm.
ToU	Time-of-use pricing.
AI	Artificial intelligence.

B. SETS

$X^{(0)}, n$	Initial sequence and index of the sequence.
$X^{(1)}, n$	Sequence obtained by accumulation of $X^{(0)}$ and index of the sequence.

The associate editor coordinating the review of this manuscript and approving it for publication was Salvatore Favuzza.

$Z^{(1)}, n$	Processed sequence of $X^{(1)}$ and index of the sequence.
$\boldsymbol{\varepsilon}^{(0)}, n$	Residual sequence and index of the sequence.
$\boldsymbol{\Delta}, n$	Relative error sequence and index of the sequence.
$\boldsymbol{L}_f$	Feasible solution set of $F(\cdot)$.

C. PARAMETERS

$\boldsymbol{B}$	Constant parameter matrix 1.
$\boldsymbol{Y}$	Constant parameter matrix 2.
a	Development coefficient.
b	Amount of grey work.
$\bar{\Delta}$	Average relative error.
$\boldsymbol{L}_b^h, \boldsymbol{h}$	State of the ESS vector and index of the vector [kW].
$\boldsymbol{G}^h, h$	Renewable energy generation power vector and index of the vector [kW].
$\boldsymbol{L}_{\text{grid}}^h, \boldsymbol{h}$	Power purchase vector of the grid and index of the vector [kW].
$\boldsymbol{L}^h, h$	Load power vector and index of the vector[kW].
$\overline{Q}^r$	Maximum charging rate of ESS [kW].
$\underline{Q}^d$	Maximum discharge rate of ESS [kW].
ξ	Comprehensive efficiency of ESS.
$SOC(t)^{h+}$	Electric quantity before discharge of ESS [kWh].
$SOC(t)^{h-}$	Electricity quantity after discharge of ESS [kWh].
$SOC_{\max}$	Maximum capacity of the ESS [kWh].
$SOC(t)$	Real-time electric quantity of the ESS [kWh].
η	Discharge depth.
$f(\cdot)$	Attenuation function capacity of the ESS.
$\boldsymbol{P}_{\text{price}}^h, \boldsymbol{h}$	Electricity price vector and index of the sequence.
$PAR(\cdot)$	Social benefit objective function.
$P_{\text{cost}}(\cdot)$	Economic benefit objective function.
$F(\cdot)$	Mapping function from decision space to objective space.
$\boldsymbol{L}_b^h, \boldsymbol{h}$	Decision vector and index of the vector [kW].
$\tilde{\boldsymbol{L}}_b^h, \boldsymbol{h}$	Arbitrary feasible solution vector and index of the vector [kW].
$F(\cdot)$	Evaluation value of particles.
ω_i^t	Inertia weights of particle i in generation t in IPSO.
$\omega_{\max}$	Maximum inertia weight in IPSO.
$\omega_{\min}$	Minimum inertia weight in IPSO.
$F_{average}^t$	Average evaluation value of the particles in PSO.
$F_{\min}^t$	Minimum evaluation value of the particles in generation t in IPSO.
$R(0, 1)$	A random value between 0 and 1.
p_t	Probability of variation at generation t in generation t in IPSO.
$p_{\max}$	Maximum variation probability in PSO.
$p_{\min}$	Minimum variation probability in IPSO.
$\boldsymbol{X}_i^t$	Particle position vector in IPSO.

D. VARIABLES

$x^{(0)}(\cdot)$	Elements in sequence $X^{(0)}$.
$x^{(1)}(\cdot)$	Elements in sequence $X^{(1)}$.
$z^{(1)}(\cdot)$	Elements in sequence $Z^{(1)}$.
$\hat{x}^{(1)}(\cdot)$	Initial predicted value of GFM.
$\hat{x}^{(0)}(\cdot)$	True Predicted Value of GFM.
$\varepsilon(\cdot)$	Elements of vector $\boldsymbol{\varepsilon}^{(0)}$.
Δ	Elements of vector $\boldsymbol{\Delta}$.
l_b^h	Charging and discharging situation of ESS in hour h [kW].
g^h	Generating situation of distributed generation equipment in hour h [kW].
l_{grid}^h	Electricity purchased from the grid in hour h [kW].
$\boldsymbol{l}^h$	Elements in vector $\boldsymbol{L}^h$ in hour h [kW].
l_{peak}	Maximum value of the element in the vector L_{grid}^h [kW].
l_{avg}	Average of the elements in the vector $\boldsymbol{L}_{\text{grid}}^h$ [kW].
l_b^h	Elements of decision vector $\boldsymbol{L}_b^h$ in hour h [kW].
x_d^+	Particle updated position in PSO.
x_d	Current particle position in PSO.

I. INTRODUCTION

The excessive use of fossil energy has caused dramatic changes in the environment [1]. To improve the energy structure of countries and deeply reduce carbon dioxide emissions [2], it has become the consensus of researchers in the power domain to absorb widely distributed renewable resources through distributed power generation equipment [3], [4]. As an important carrier of renewable energy production and use, the energy storage system (ESS) can realize the time-space shift of renewable energy [5], stabilize the fluctuation of load, reduce the cost of electricity [6], and improve the local consumption capacity of renewable energy [7]. However, ESS has the characteristics of high investment cost and long return period, resulting in low enthusiasm of investors and only taking a wait-and-see attitude. Therefore, it is of great significance to deeply explore the benefits brought by ESS [8] and provide more comprehensive data support for the configuration of ESS capacity to improve the enthusiasm of investors and promote the low-carbon transformation of the world energy system [9].

ESS can make loads schedulable, so current research is mainly focused on the joint management of loads through joint scheduling of energy storage distributed generation systems [10]. Compared to traditional methods of

generating revenue by scheduling changes in certain loads, the benefits are higher. Specifically, traditional scheduling only involves dispatchable loads, such as cold water [11], water heaters [12], and air conditioners [13], which have significant limitations. Excessive scheduling of such loads will seriously affect user comfort. Therefore, relevant researchers attempt to schedule without changing the user's electrical appliances through ESS. Jalali and Alizadeh-Mousavi [14] present a rolling horizon optimal energy management mechanism using real-time grid monitoring data. Scheduling through ESS after forecasting the load reduces the peak load, improves renewable energy utilization, and reduces carbon emissions. Literature [15] presents a model for the energy management system of a building microgrid coupled with battery energy storage and reduced electricity costs. Although the above studies have conducted an in-depth analysis of the benefits brought by ESS [14], [15], there is little mention of the impact of ESS-related parameters on benefits [14]. In fact, the biggest impact factor on benefits is the capacity of the ESS.

A redundancy of parameters will cause a waste of resources, and overly conservative parameters can hardly achieve the ideal optimization effect. Scholars usually set the goal as the lowest construction cost [16], the lowest operation cost [17], and the lowest system operation fluctuation [18], to provide a basis for the parameter configuration of ESS. Compared with single-objective optimization. Multi-objective optimization can utilize the degree of freedom in the process of single-objective optimization to improve other optimization objectives. Leone et al. [19] took emissions and costs as objectives and optimized the battery capacity by transforming linear weighting into single-objective optimization. Simplifies the difficulty of solving multi-objective optimization problems; but reduced the reliability of the solution. Literature [20] establishes a multi-objective function based on economy and accessibility of power equipment capacity. Celik et al. [21] proposed an energy management and sharing strategy. Showing good performance in reducing costs and peak load; Mansouri et al. [22] establish a multi-objective optimization function, which improves the three objectives of operating cost, emissions, and peak-to-average load ratio. In the process of optimization, user satisfaction is also considered. Thirugnanam et al. [23] proposed an optimization model aimed at minimizing the power cost and maximizing the reliability coefficient of a hybrid AC/DC microgrid solved by a multi-objective particle swarm optimization algorithm (MOPSO). Numerical simulation shows the effectiveness of the proposed strategy. References [24] and [25] consider user privacy protection while optimizing multiple objectives. Although privacy protection does not provide intuitive economic benefits, it can motivate users and make the proposed strategy easier to implement [22], [24], [25]. The above research improves the performance of other targets based on single-target optimization and further exploits the benefits brought by ESS [19], [20], [21], [22], [23].

In addition, the load characteristics change has a great impact on the benefits generated. Considering the great difference of load characteristics under different scenarios, some scholars have explored more scenarios to comprehensively improve the economic and social benefits brought by ESS. Specifically, these researchers will consider various uncertain factors or the benefits of switching between different work scenarios. Zhao et al. [26] optimized the ESS capacity in two scenarios of grid connection and island operation of the microgrid, resulting in an improved economy of the microgrid system. And verified that under the established model, the performance of AEO is better than that of the particle swarm optimization algorithm (PSO) Moreover, due to the fast response ability of the ESS, the primary frequency modulation ability of the microgrid during island operation has been improved. Nguyen et al. [27] explored the address and capacity of ESS by adopting the artificial ecosystem optimization (AEO) algorithm. Through the analysis of three different test scenarios, the power purchase cost of the grid was reduced. Xie et al. [28] established a bi-level mixed-integer nonlinear programming model and solved the mathematical model efficiently with the original decomposition coordination algorithm based on dual decomposition and alternative iteration strategy. Provide support for obtaining the optimal capacity of ESS under different scenarios. In [29] and [30], researchers also analyzed many scenarios in a short period, obtained good optimization results, and verified the reliability of the conclusions through real data simulation. Although the above research has achieved relatively ideal results, and broadened the application scenarios of ESS, there are certain drawbacks. Simultaneous optimization of multiple objectives means high computational complexity, which further leads to a more complex optimization process and difficulty in obtaining a complete solution set [19], [20], [21], [22], [23], [27]. In [31] and [32], this phenomenon is more reflected in the edge of the non-dominant solution set, which means that we cannot discuss the optimal benefit of each goal. This problem can also be encountered when converting a multi-objective optimization problem into a single-objective optimization problem using a linear weighting method [19], [33]. If the weight of an objective becomes zero, the problem will degenerate into a single objective problem. There is still no unified conclusion on the selection of weights for each target [32]. Moreover, the above research only considers the load change in a short period [13], [16], [21], [22], or only analyzes a few scenarios [17], [26], [27] represented by typical data in recent two years, and does not consider the dynamic characteristics of the load in the life cycle of distributed power generation equipment [28], [29], [30], [34]. This does not provide comprehensive data support for the configuration of ESS capacity. Therefore, it is very important to consider the change of load over a long-time span for the capacity configuration of ESS.

In this work, we propose a Long-term ESS capacity configuration method based on the Improved Grey Forecasting

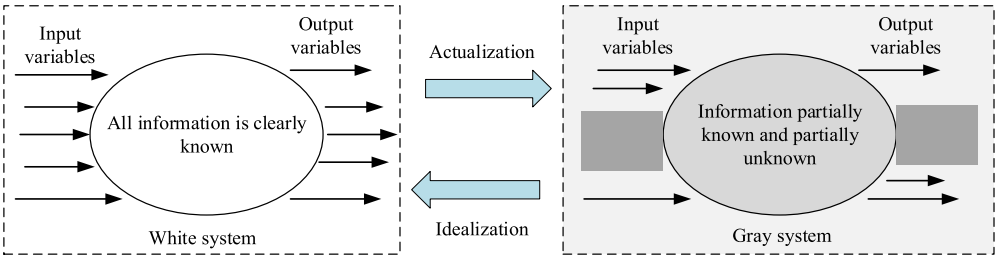

FIGURE 1. White system and grey system.

Model (IGFM). The main contributions of this paper can be summarized as follows:

1) This study improves the basic grey forecasting model to make it more accurate.

2) This paper proposes a new hierarchical scheduling method that can maximize social benefits while ensuring maximum economic benefits. At the same time, compared with the multi-objective optimization method, its complexity is lower.

3) We have conducted an in-depth analysis of the ESS yield under different life cycles and capacity sizes, which has greatly reduced the error between expected and actual returns over a long-time span.

The rest of this paper is organized as follows: In the second part of this paper, we introduce the grey theory and establish a dynamic forecasting model based on the grey theory and a scheduling model. In the third part, the whole forecasting model is improved and the hierarchical scheduling algorithm is introduced. The fourth part is the simulation results. The conclusions and some prospects are put in the last chapter.

II. MATHEMATICAL MODEL

A. GREY SYSTEM THEORY AND FORECASTING MODEL

In the second half of the 20th century, with the development of system science, people found that the amount of information available in the system was very limited. The emergence of fuzzy sets, rough sets, and gray system theory [35] provided a way to solve this problem. Among them, the grey system theory proposed by Professor Deng Julong has been widely applied in various fields and widely accepted by most international journals [36].

As shown in Figure 1. a grey system is defined as a system with grey inputs and outputs, which is characterized by a lack of information and large uncertainty, and extremely limited data obtained. The greatest contribution of the grey system theory is that it can establish the grey dynamic model of the main behavior characteristic quantity and correlation factor of the system through mathematical methods. It plays an important role in analyzing the development trend of the system, deeply mining grey information, helping decision-makers make correct decisions, and controlling the development of the system in the right direction.

GFM can be divided into first-order univariate model GM (1,1) and first-order multivariable dynamic model GM (1, N), among which GM (1,1) is more classical and more widely used. The establishment of the GM (1,1) model is mainly divided into the following steps:

1. Data preprocessing. Represent the collected raw data in the form of number sequence, and conduct preliminary data processing.

$$X^{(0)} = \left\{x^{(0)}(1), x^{(0)}(2), \cdots, x^{(0)}(n)\right\} \tag{1}$$

$$X^{(1)} = \left\{x^{(1)}(1), x^{(1)}(2), \cdots, x^{(1)}(n)\right\} \tag{2}$$

$$Z^{(1)} = \left\{z^{(1)}(2), z^{(1)}(3), \cdots, z^{(1)}(n)\right\} \tag{3}$$

Equation (1) is the sequence form of information collected, which is called the original data sequence; (2) is the cumulative form of (1), $X^{(1)}$ also called the 1-AGO $X^{(0)}$ sequence; (3) is the nearest neighbor mean the sequence of (2), also known as the background value. The elements in the formula meet the following relationships:

$$x^{(1)}(k) = \sum_{i=1}^{k} x^{(0)}(i), \quad k = 1, 2, \cdots, n \tag{4}$$

$$z^{(1)}(k) = \frac{1}{2}\left[x^{(1)}(k) + x^{(1)}(k-1)\right], \quad k = 2, 3, \cdots, n \tag{5}$$

2. Form GM (1,1) basic model and albino differential equation. The basic form of GM (1,1) can be obtained by combining Formula (1)-(5), as shown in (6). The differential equation model (albino differential equation) is shown in (7) [36]. In the following part, we can use Equation (6) to solve the parameter a b, and then use (7) to solve the predicted value.

$$x^{(0)}(k) + az^{(1)}(k) = b, \quad k = 2, 3, \cdots, n \tag{6}$$

$$\frac{dx^{(1)}(k)}{dk} + ax^{(1)}(k) = b, \quad k = 1, 2, \cdots, n \tag{7}$$

3. Solve model parameters a and b. The least squares method can be used to solve the problem. Assume that the matrix formed by parameter ab is $\hat{\boldsymbol{a}} = [a, b]^T$, and construct the parameter matrix $\boldsymbol{B}\ \boldsymbol{Y}$ (Eq. 8). At this time, (6) can be further organized into the form of (9). The elements in the matrix $\boldsymbol{B}\ \boldsymbol{Y}$ are known constants, and the estimated value a b

of the undetermined model can be solved by (10).

$$\boldsymbol{B} = \left[-\boldsymbol{Z}^{(1)}, \boldsymbol{E}\right] = \begin{bmatrix} -z^{(1)}(2) & 1 \\ -z^{(1)}(3) & 1 \\ \vdots & \vdots \\ -z^{(1)}(n) & 1 \end{bmatrix}, \quad \boldsymbol{Y} = \begin{bmatrix} x^{(0)}(2) \\ x^{(0)}(3) \\ \vdots \\ x^{(0)}(n) \end{bmatrix} \tag{8}$$

$$\boldsymbol{Y} = \boldsymbol{B}\hat{\boldsymbol{a}} \tag{9}$$

$$\hat{\boldsymbol{a}} = \left(\boldsymbol{B}^T\boldsymbol{B}\right)^{-1}\boldsymbol{B}^T\boldsymbol{Y} \tag{10}$$

4. Solve the whitening differential equation (Eq. 7), and restore the predicted value with (4). The solution of the whitening differential equation and the recovery process of the predicted value is shown in (11), (12).

$$x^{(1)}(k) = \left[x^{(0)}(1) - \frac{b}{a}\right]e^{-ak} + \frac{b}{a}, \quad k = 1, 2, \cdots, n \tag{11}$$

$$\begin{aligned} \hat{x}^{(0)}(k+1) &= \hat{x}^{(1)}(k+1) - \hat{x}^{(1)}(k) \\ &= (1 - e^{a})(x^{(0)}(1) - \frac{b}{a})e^{-ak}, \quad k = 1, 2, \cdots, n \end{aligned} \tag{12}$$

The above is the whole process of establishing and solving the GM (1,1) model. The error between actual data and simulation data is the best method to test whether the model is effective.

Define residual sequence:

$$\begin{aligned} \boldsymbol{\varepsilon}^{(0)} &= \{\varepsilon(1), \varepsilon(2), \cdots, \varepsilon(n)\} \\ &= \{x^{(0)}(1) - \hat{x}^{(0)}(1), x^{(0)}(1) - \hat{x}^{(0)}(2), \\ &\quad \cdots, x^{(0)}(n) - \hat{x}^{(0)}(n)\} \end{aligned} \tag{13}$$

Then the relative error sequence can be expressed as:

$$\begin{aligned} \boldsymbol{\Delta} &= \left\{\left|\frac{\varepsilon(1)}{x^{(0)}(1)}\right|, \left|\frac{\varepsilon(2)}{x^{(0)}(2)}\right|, \cdots, \left|\frac{\varepsilon(n)}{x^{(0)}(n)}\right|\right\} \\ &= \{\Delta_1, \Delta_2, \cdots, \Delta_n\} \end{aligned} \tag{14}$$

The average relative error can be expressed as:

$$\bar{\Delta} = \frac{1}{n-1}\sum_{i=2}^{n}\left|\frac{\varepsilon(i)}{x^{(0)}(i)}\right| \tag{15}$$

Because historical observation data is limited and highly discrete, and meteorological data has been seriously lost, long-term load forecasting with partial load data is a typical grey system. Therefore, GFM is established through grey system theory to predict load change trends, and then the accuracy of the model is verified through the analysis of relative error and average error. Compared with the artificial intelligence (AI) prediction method [37], [38] which requires a lot of data training, it has the advantage of less dependence on the amount of data. In addition, there is no evidence that complex methods are better than simple methods [39]. Note that the AI-based methods take a long time to calculate during training positioning, so they are not suitable for some scenarios.

B. DISPATCHING MODEL OF LOAD AND ESS

Take a day as a cycle and every hour as the time granularity for discretization. The working state of the ESS, the level of renewable energy generation, the power purchase of the grid, and the load power consumption can be expressed as a set of vectors with a length of 24, as shown in (16)-(19):

$$\boldsymbol{L}_b^h = [l_b^1, \ldots, l_b^H] \tag{16}$$

$$\boldsymbol{G}^h = \left[g^1, \ldots, g^H\right], \quad g^h \geq 0 \tag{17}$$

$$\boldsymbol{L}_{\text{grid}}^h = [l_{\text{grid}}^1, \ldots, l_{\text{grid}}^H], \quad l_{\text{grid}}^h \geq 0 \tag{18}$$

$$\boldsymbol{L}^h = \left[l^1, \ldots, l^H\right], \quad l^h \geq 0 \tag{19}$$

At the same time, the operation status of the ESS shall satisfy the constraints of charge/discharge rate, efficiency, capacity, power balance, charge/discharge depth, and battery aging. The expression is shown in (20)-(25):

$$0 \leq l_b^h \leq \overline{Q}^r \tag{20}$$

$$-\underline{Q}^d \leq l_b^h \leq 0 \tag{21}$$

$$SOC(t)^{h+} - SOC(t)^{h-} = \xi l_b^h \tag{22}$$

$$\boldsymbol{L}_{\text{grid}}^h = \boldsymbol{L}^h + \boldsymbol{L}_b^h - \boldsymbol{G}^h \tag{23}$$

$$\eta SOC_{\max} \leq SOC(t) \leq SOC_{\max} \tag{24}$$

$$SOC_{\max}^{re} = SOC_{\max}(1 - f(t)) \tag{25}$$

Then, combined with the time-of-use (ToU) pricing, two objective functions are established. The first objective function is to minimize the user's electricity cost, and the second objective is to achieve the highest social benefits. The social benefit can be expressed as the value of stabilizing the load fluctuation, thereby reducing the operating pressure of the power grid. In this paper, it is defined as the peak-to-average ratio (PAR) of the power exchanged with the power grid. These two objectives can be expressed as:

$$PAR(\boldsymbol{L}_b^h) = \frac{l_{\text{peak}}}{l_{\text{avg}}} = \frac{\max l_{\text{grid}}^h}{\frac{1}{H}\sum_{h=1}^{H} l_{\text{grid}}^h} \tag{26}$$

$$P_{\text{cost}}(\boldsymbol{L}_b^h) = \boldsymbol{L}_{\text{grid}}^h\left(\boldsymbol{P}_{\text{price}}^h\right)^T \tag{27}$$

It should be noted that the status of these two goals is not equal. To maximize the interests of users, we need to take (28) as the primary goal of optimization. After achieving the maximum economic benefits, we will consider improving social benefits, which will help to improve the enthusiasm of investors. The final scheduling model can be expressed as:

$$\begin{cases} \min\ \boldsymbol{F}(\boldsymbol{L}_b^h) = (PAR(\boldsymbol{L}_b^h), P_{\text{cost}}(\boldsymbol{L}_b^h))^{\text{T}} \\ s.t.\ P_{\text{cost}}(\boldsymbol{L}_b^h) \leq P_{\text{cost}}(\tilde{\boldsymbol{L}}_b^h), \quad \forall \tilde{\boldsymbol{L}}_b^h \in \boldsymbol{L}_f \\ \quad (21)(22)(23)(24)(25)(26) \end{cases} \tag{28}$$

III. IMPROVEMENT AND SOLUTION OF THE MODEL

A. IMPROVEMENT AND SOLUTION OF GFM

The degree of coincidence between GFM and real data depends on the relative error. Considering the randomness

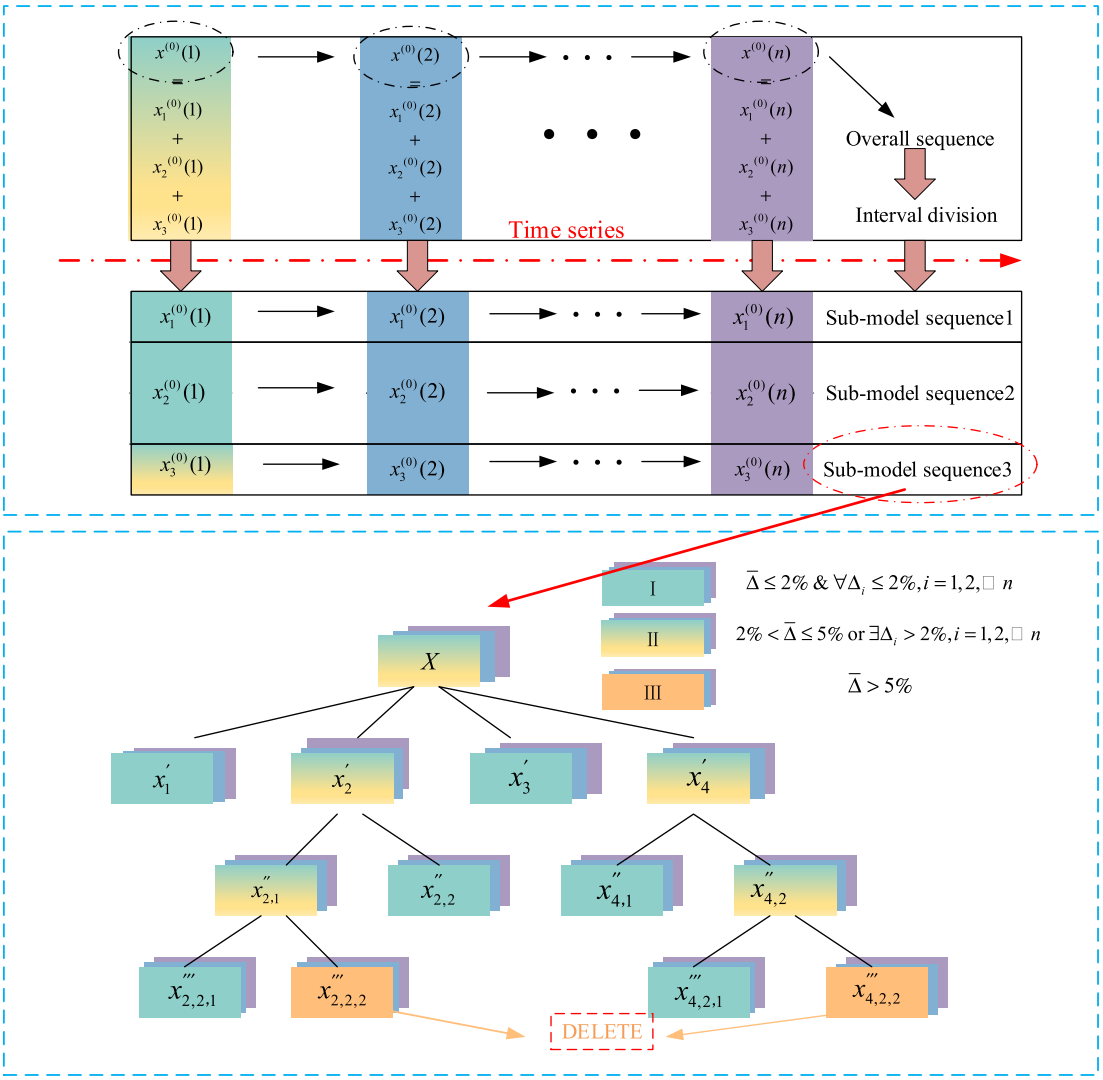

FIGURE 2. Schematic diagram of IGFM.

and volatility of the load, it is very difficult to accurately predict the specific changes of the load every day. Therefore, we only need to ensure that the load is accurate in most cases, ignoring the cases with fewer occurrences and larger fluctuations, to ensure the reliability of the conclusions.

Considering the obvious periodicity of load change, the annual load is decomposed into a seasonal load, and the seasonal load is taken as the sub-model of the load forecasting model. When the load has a large deviation, the time interval continues to be divided until the abnormal load is found and eliminated. At this time, each sub-model contains a pair of independent development coefficients and grey action quantities for our selection. Its conceptual diagram is shown in FIGURE 2.

According to the size of relative error and average error, we divide the sub-models into three categories, namely, the accurate model, the minor error model, and the abnormal model. Specific standards are shown in TABLE 1.

TABLE 1. Load division standard.

Types	Conditions
I	$\bar{\Delta} \le 2\% \ \& \ \forall \Delta_i \le 2\%, i = 1,2,\mathrm{L}\ n$
II	$2\% < \bar{\Delta} \le 5\% \text{ or } \exists \Delta_i > 2\%, i = 1,2,\mathrm{L}\ n$
III	$\bar{\Delta} > 5\%$

Then, the corresponding GM (1,1) model and albino differential equation should be modified to the form of 29,30. The specific solution method has not changed, but the obtained model will have a set of mutually independent development coefficients and grey work amount, and the error will be greatly reduced compared with the original model.

$$\begin{cases} x_1^{(0)}(k) + a_1 z_1^{(1)}(k) = b_1, & k = 2, 3, \cdots, n \\ x_2^{(0)}(k) + a_2 z_2^{(1)}(k) = b_2, & k = 2, 3, \cdots, n \\ \cdots \\ x_j^{(0)}(k) + a_j z_j^{(1)}(k) = b_j, & k = 2, 3, \cdots, n \end{cases} \tag{29}$$

$$\begin{cases} \dfrac{dx_1^{(1)}(k)}{dk} + a_1 x_1^{(1)}(k) = b_1, \quad k = 1, 2, \cdots, n \\ \dfrac{dx_2^{(1)}(k)}{dk} + a x_2^{(1)}(k) = b_2, \quad k = 1, 2, \cdots, n \\ \cdots \\ \dfrac{dx_j^{(1)}(k)}{dk} + a_j x_j^{(1)}(k) = b_j, \quad k = 1, 2, \cdots, n \end{cases} \tag{30}$$

Finally, after obtaining the long-term load change trend, the load can be increased proportionally in combination with the typical load curve to obtain the future long-term load curve.

Note: We did not consider the growth of renewable energy in the simulation process, because there is no obvious change trend of renewable energy in each cycle, only the number of days in a year changes.

B. SCHEDULING MODEL SOLUTION

Based on the above part of load forecasting, we designed an interesting solution to the scheduling model. The method concept diagram is shown in FIGURE 3. Firstly, the improved particle swarm optimization (IPSO) algorithm is used to solve the optimal economic objective. After obtaining the optimal economic dispatch vector. The time intervals are divided according to the working state of the ESS and the ToU pricing period. Since the pricing and the charging and discharging state of the ESS has not changed within the interval, the change of economic benefits will not be affected while the power exchange with the grid is smooth. When smoothing the power exchange, we use the Lagrange multiplier method (LMM).

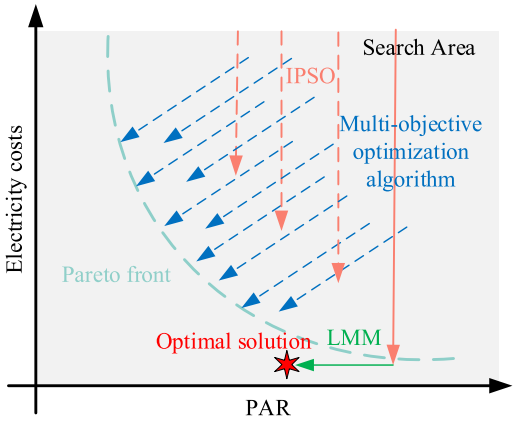

FIGURE 3. Scheduling model-solving concept diagram.

Since particle swarm optimization (PSO) is a heuristic algorithm, there are problems with convergence accuracy and speed, so we have improved the basic particle swarm algorithm. The changes are as follows:

To increase the particle optimization speed, the inertia weight is dynamically updated according to the evaluation value of the current particle. The updated formula is as follows:

$$\omega_i^t = \begin{cases} \omega_{\max}, & if\ F(\boldsymbol{X}_i^t) > F_{\text{average}}^t \\ \omega_{\min} + (\omega_{\max} - \omega_{\min}) \dfrac{F(\boldsymbol{X}_i^t) - F_{\min}^t}{F_{\text{average}}^t - F_{\min}^t}, & \\ else & \end{cases} \tag{31}$$

To ensure particle diversity, avoid serious aggregation of particles in the later stage, and fall into local optimization, we refer to the mutation operation of GA. Each time the position is updated, we randomly select an element in the particle position vector for mutation operation. The mutation formula is:

$$x_d^+ = x_d + x_d R(0, 1) \tag{32}$$

Whether the particle will mutate depends on the mutation probability. In this paper, we adopt the linearly increasing mutation probability, which can be expressed as:

$$p_t = p_{\min} + (p_{\max} - p_{\min})(t \div T) \tag{33}$$

TABLE 2. Pseudocode for scheduling model solution.

Algorithm: Scheduling model solving

Input data: load data obtained from IGFM

(S.1) Set particle swarm parameters, iteration number t=0, initialize particle position, obtain current particle position, and calculate particle evaluation value.

(S.2) Update the particle inertia weight according to Formula 29, update the particle position, and calculate the particle evaluation value. t=t+1.

(S.3) Perform particle mutation operation according to (32) and (33), and update the position of mutation particles.

(S.4) If the iteration termination condition is met GO TO (S.5)

Else go to（S.2）

(S.5) Interval division, and maximize social benefits through the Lagrange multiplier method

(S.6) Repeat the above process until all the output data of the IGFM are calculated.

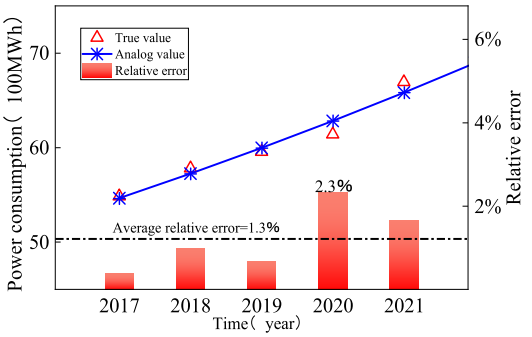

FIGURE 4. Prediction effect of basic GFM.

IV. SIMULATION ANALYSIS

In this section, we verify the accuracy and reliability of the proposed algorithm and model through simulation results and

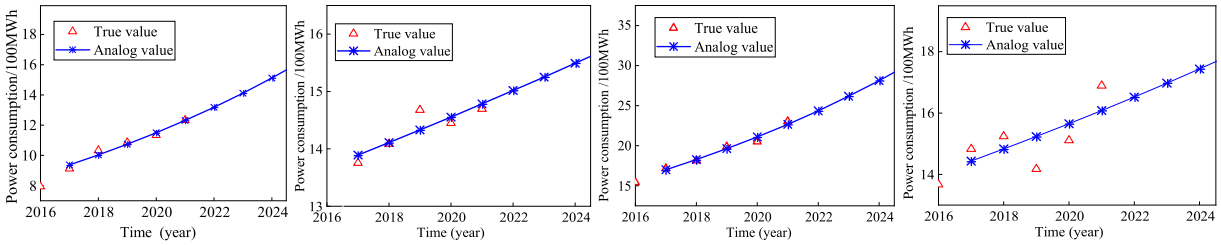

FIGURE 5. Prediction effect after interval division. (Spring, Summer, Autumn, and Winter.)

TABLE 3. Error comparison between GFM and IGFM.

Region	Time	Original data		Analog value		Residual		Relative error	
		GFM /MWH	IGFM /MWH	GFM /MWH	IGFM /MWH	GFM /MWH	IGFM /MWH	GFM	IGFM
Summer	2017	1375.5	1245.7	1389.1	1256.8	-13.6	-11.1	0.99%	0.89%
	2018	1408.6	1301.5	1410.9	1290.2	-2.3	11.3	0.16%	0.87%
	2019	1467.9	1332.1	1433.1	1324.5	34.8	7.6	2.37%	0.57%
	2020	1445.0	1354.7	1455.5	1359.7	-10.5	-5	0.73%	0.37%
	2021	1469.7	1393.5	1478.4	1395.8	-8.7	-2.3	0.59%	0.17%
Winter	2017	1483.2	1302.4	1443.5	1302.7	39.7	-0.3	2.68%	0.02%
	2018	1523.9	1352.5	1483.1	1341.6	40.8	10.9	2.68%	0.81%
	2019	1417.5	1372.2	1523.7	1381.7	-106.2	-9.5	7.49%	0.69%
	2020	1511.0	1412.5	1565.4	1422.9	-54.4	-10.4	3.60%	0.74%
	2021	1689.1	1475.3	1608.3	1465.4	80.8	9.9	4.78%	0.67%

explore the changing trend of the ESS optimization effect under different capacities over a long-time span.

A. SIMULATION OF PREDICTION EFFECT OF GFM AND IGFM

Based on the 6 years of Chinese community load data, we use the basic GFM to simulate and forecast the load data within the span. The simulation results are shown in FIGURE 5.

It can be seen from FIGURE 4 that the grey prediction model has a good prediction effect. However, in 2020, there was a large error (the error was 142.6 MWh), the relative error was 2.3%, and the average relative error was 1.2%, belonging to the second type of model. Although the average error is small, for the effect of long-term prediction, the error is likely to increase with time.

In addition, considering that the load has different growth characteristics in different periods, it is less reliable to express the changing trend in the whole cycle with one model. Therefore, we divide the time interval, obtain the load data of the four seasons, and predict to get FIGURE 6.

It can be seen from FIGURE 5 that the prediction deviation in spring, summer, and autumn is obviously smaller than that in winter, and the average relative error is 1.63%, 0.96%, and 1.42% respectively. The average relative error in winter is 4.25%, which is difficult to be directly applied and needs to be treated with an improved model. In addition, we found that the load error in the summer of 2019 was 34.8MWh, and the relative error was 2.37%. Therefore, spring and autumn are the first type of models that can be directly applied, while winter and summer are the second types of models that need

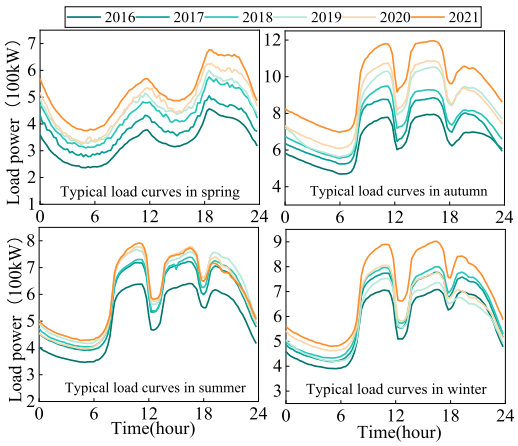

FIGURE 6. Typical load curves in different seasons and years.

to be further treated with IGFM. After IGFM processing, we get TABLE 3. It can be seen that the average relative error of the winter load is reduced from 4.25% to 0.59%, and the summer load is not only reduced to 0.57%, but the error of each prediction data is within 1%.

To verify the feasibility of using GFM to obtain long-span load data, we extracted the characteristics of each quarterly load in the past six years and finally obtained 24 typical daily load curves, as shown in FIGURE 6. It can be seen that the load change regularity shows obvious seasonal characteristics, and the trend is consistent. The load of the same season in different years only changes in proportion. This also proves that we only need to obtain the load change coefficient to infer the typical load data in a long-time span in the future.

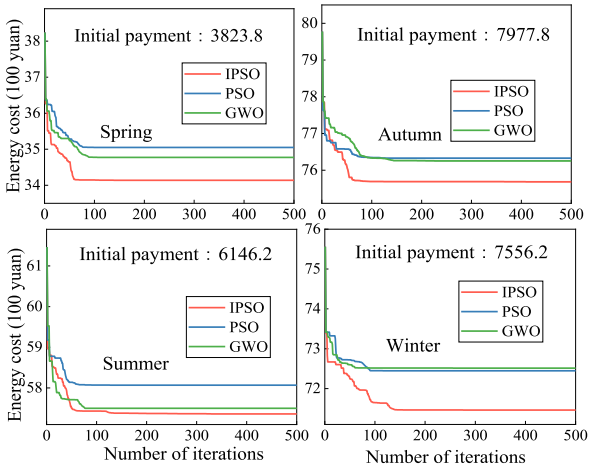

FIGURE 7. Payment iteration process.

TABLE 4. Electricity price parameter.

Time interval	Electricity Price(yuan/kWh)	Electricity Price level
0.00-9.00	0.19	Valley
9.00-12.00	0.62	Flat
12.00-15.00	0.98	Peak
15.00-20.00	0.62	Flat
20.00-24.00	0.98	Peak

TABLE 5. The parameter of IPSO.

Parameter	Symbol	Value
Population quantity	--	100
Max-inertia weight	ω_{max}	0.9
Min-inertia weight	ω_{min}	0.4
Max-Mutation Rate	p_{max}	0.3
Min-Mutation Rate	p_{min}	0.05
Iterations	--	500

In addition, we can see that the load growth in each season is not the same. For example, in spring, the load growth is approximately linear, while other growth trends need to be specifically analyzed. It also shows that IGFM is more targeted and reliable than GFM in prediction. Later in Section IV-C, we will verify the accuracy of this method based on the error between the predicted data and the real data.

It should be noted that the research results will vary in different periods and regions. For example, the different development stages of a country (or different regions on the earth) will have great differences. And it can be seen from FIGURE5 and FIGURE 6 that there are obvious differences in the change of load characteristics for different times. The specific performance is that the increase in spring and autumn is smoother, and the change in summer and winter is more complex. Based on this, the research cases in this paper have certain time and space dependence and need to be more strictly verified for different times and different regions.

TABLE 6. The parameter of ESS.

Parameter	Symbol	Value
Capacity	SOC_{max}	500kWh
Charge efficiency	ξ	0.95
Charge /discharge rate	$\overline{Q}^r$ / $-\underline{Q}^d$	100kW
Depth of discharge	η	0.1

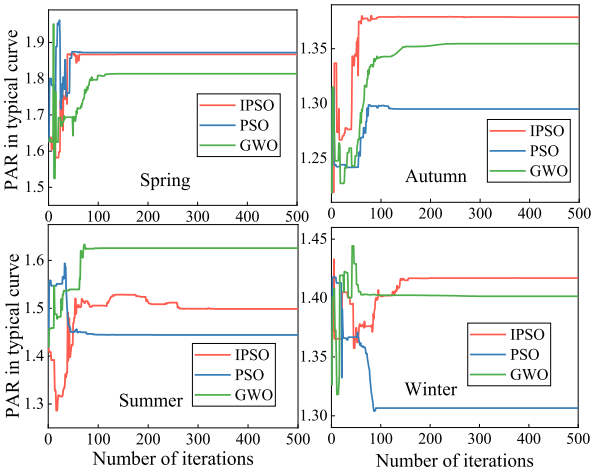

FIGURE 8. PAR iteration process.

B. SCHEDULING MODEL SIMULATION

To verify the effectiveness of the scheduling algorithm, we take the typical load data of the fourth quarter of 2016 as an example and combine the ToU pricing policy of a place in China to schedule. The specific electricity price parameters are shown in TABLE 4. IPSO iteration parameter settings are shown in TABLE 5. Refer to TABLE 6 for ESS parameters. Then, FIGURE 8 is obtained through simulation.

To make an effective comparison, we set grey wolf optimization (GWO) and PSO as the control group for simulation, and the population number of both is 100.

It can be seen from FIGURE 7 that PSO and GWO converge slowly, and both fall into the situation of local optimization. The convergence speed of IPSO is significantly faster than that of GWO and PSO, and the accuracy of IPSO in 50 iterations is equivalent to that of PSO and GWO in 100 generations. And due to the adaptive mutation function of IPSO, the convergence accuracy still improved slightly during the 100 to 400 generations and finally converged to 3413.7, 5736.1, 7567.7, 7146.1 yuan, which was 10.8%, 7.7%, 4.9%, 5.6% lower than the initial payment. The effect of reducing payment was significantly better than PSO and GWO, which proved the effectiveness of IPSO. To increase the statistical significance, we randomly generated 40 groups of large disturbance data and carried out simulation optimization as shown in FIGURE 9.

It can be found that after the sample data is expanded, due to the large dependence of the heuristic algorithm on the initial value of iteration, the partial numerical convergence of

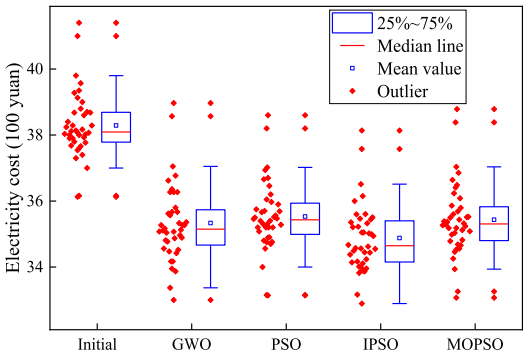

FIGURE 9. Disturbance data simulation results.

GWO and PSO is also ideal. In addition, due to complexity issues, MOPSO is also similar to GWO and PSO in reducing power consumption costs. However, overall, the convergence accuracy of the optimization algorithm proposed in this paper is still significantly improved compared with other optimization algorithms.

In the first optimization process, although the power cost was reduced by adjusting the load from the peak period to the valley period, the PAR of the load was not set with relevant optimization goals, so it showed an unstable trend in the early iteration (fig 8). With the increase in the number of iterations, the PAR was not improved. Therefore, we have carried out a secondary optimization, and the optimization effect is shown in FIGURE 10.

It can be seen from FIGURE 10 that after optimized dispatching, ESS has played a role in cutting peak and filling the valley, thus reducing the power cost. At the same time, renewable energy is fully absorbed by distributed generation equipment, which improves the penetration rate and local absorption capacity of renewable energy. The PAR of the load is reduced from 1.727, 1.494, 1.373, and 1.496 optimized for the first time to 1.487, 1.412, 1.253, and 1.39, respectively by 14.7%, 5.5%, 8.87%, and 7.1%. Moreover, after the second optimization, it is verified by calculation that the economic benefits have not decreased due to the second optimization.

This method is worth promoting in reality. Firstly, due to the fast response capability of ESS, technical support is provided for implementing this scheduling method. Secondly, intelligent optimization algorithms have a faster computational speed and can meet the requirements of making decisions in a very short time to cope with more complex situations.

C. CAPACITY CONFIGURATION OF ESS

With the above parameters as the standard, we have made scheduling simulations and statistics under a long-time span based on IGFM prediction data. In the process of simulation, we also considered battery aging factors. The simulation results are shown in FIGURE 11.

As can be seen in FIGURE 11. a, in a long-time span, the economic benefits (rate of return) generated by ESS with different capacities do not show a simple linear relationship, but the rate of return will gradually decline with the change of load characteristics and battery aging, and the decline speed will gradually slow down. Taking the benefits under the capacity of 600 kWh as an example, the benefit in 2016 is 7.24%, which will be reduced to 4.48% and 3.35% in 2022 and 2027, respectively, by 38.1% and 53.7%. If only the current data is used as the data support for capacity configuration, the rate of return will have a large deviation in the service life. At the same time, in the figure, we compared the profit effect of the real data from 2016 to 2022 and found that the gap between the gray prediction simulation data and the real data is within 0.2%.

As can be seen in FIGURE 11. b, the average rate of return under different capacities increases with the increase of ESS capacity, but the growth trend gradually slows down. In different service cycles, the trend is similar, but it should be noted that the average benefits generated in different service cycles are not evenly distributed. For example, in 400kwh capacity, the ESS service life has achieved an average optimization effect of 5.01%, 4.58%, 4.21%, and 3.92% respectively in 3, 6, 9, and 12 years. At this time, we configure the parameters of ESS with the expected rate of return of 4.5%, and the capacity will be at least 351, 397, 455, and 526 kWh in the life cycle of 3, 6, 9, and 12 years. If only the data from 2016 is used for reference, the capacity will be 304 kWh. The deviation of the rate of return from the expected value will reach 10.9%, 17.8%, 24.4%, and 30.6% respectively. As shown in FIGURE 11. c if the expected return rate is 3.5%, 3.5%, or 4%, there will also be large errors, which also proves the effectiveness of the proposed allocation method, which also proves the effectiveness of the proposed parameter configuration method.

As shown in FIGURE 11. d and FIGURE 11. e, the social benefits obtained show an increasing trend (PAR decreases) with the change of load characteristics and show a small correlation with the capacity. However, when the capacity of ESS is large, the PAR will increase. This is because when the capacity is large, the degree of freedom of two-stage optimization will be compressed, thus reducing the effect of two-stage optimization. As the peak load and renewable energy offset each other, PAR will decrease over time.

This result has certain theoretical and practical value. First, it decomposes the optimization process of multiple objectives and reduces the complexity of the solution. Compared with the works of literature [19], [20], [21], [22], [23], [31], and [32], it avoids the impact of the inadequate non-dominated solution set on the analysis results. Secondly, in the process of optimization, this article takes into account the change of yield with the increase in the period, which can provide more comprehensive data support for the capacity configuration of ESS. For example, in [22] and [31], the economic benefits achieved are 16% and 22.2%, but with the growth of the period (6 years, 9 years), there will be a large deviation. As shown in FIGURE 11 f, under the conditions of this paper, the yield may be reduced to 13.3% and 18.4% (6 years), 11.3%, and 15.76% (12 years).

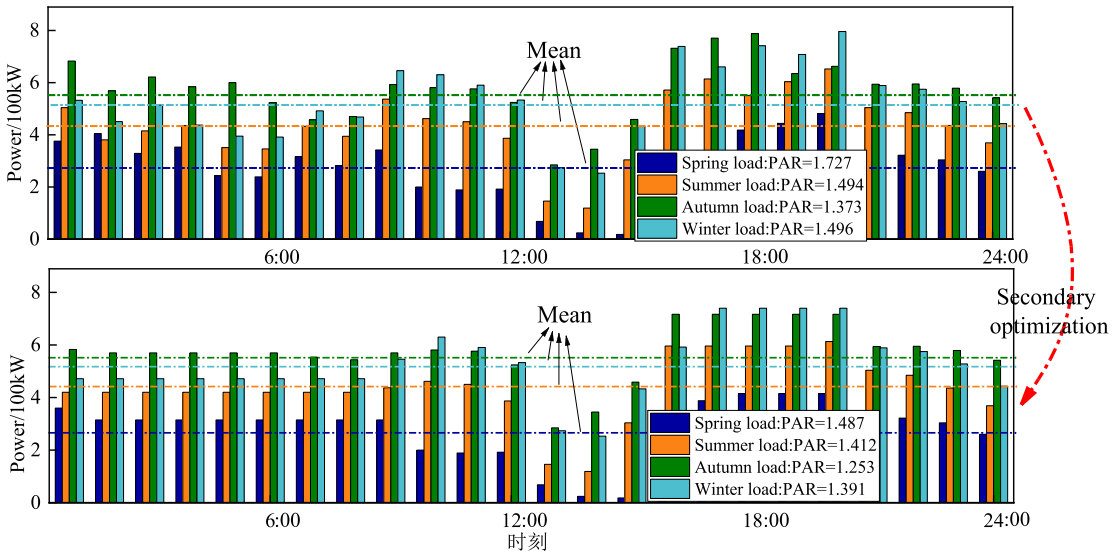

FIGURE 10. Load curve after secondary optimization.

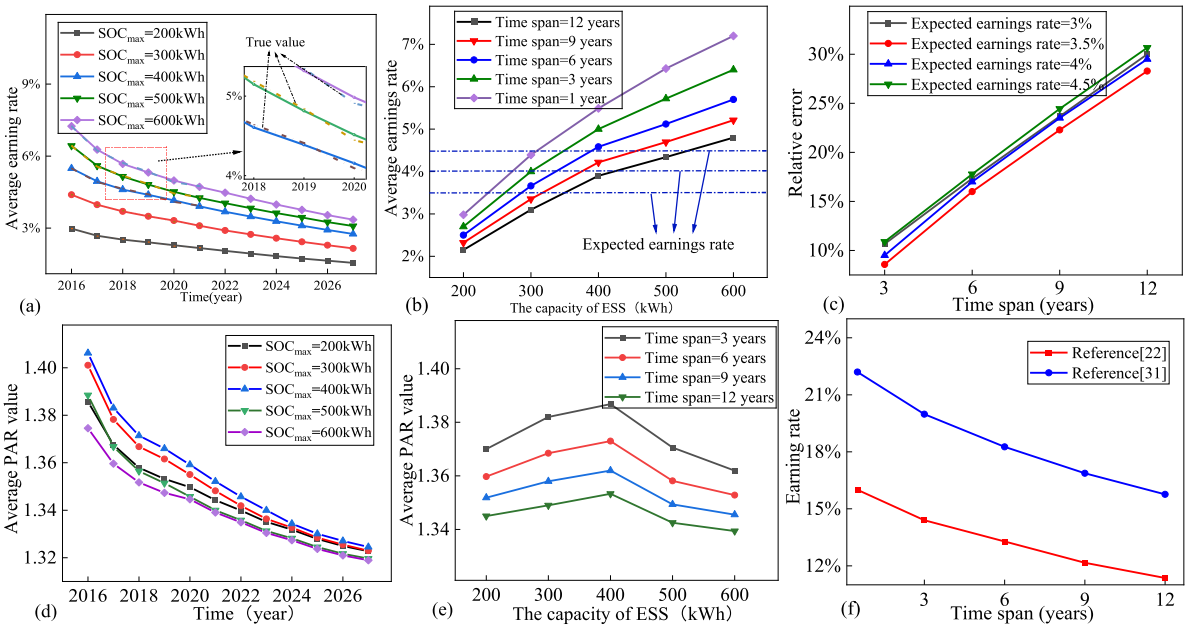

FIGURE 11. Comparison of optimization effects of different periods and capacities. a. The return rate under the different capacities of ESS. b. Average rate of return for different service life under the different capacities of ESS. c. The error between different periods and the expected rate of return. d. PAR optimization effect of different capacities of ESS. e. Average PAR of different capacities in different periods. f. earning rate change curve in literature [22] and [31].

To verify the generalizability of the conclusions, we performed simulations for the other three regions (Case 4 is the above case, and case 1,2,3 for the rest, respectively) and plotted the simulation results in Figure 12.

As can be seen in FIGURE 12, there is some variation in the error over a long-time span in different regions, for example, the relative error in case 2 is small (minimum value of 3.3%), while the error in case 4 is large (maximum value of 29.6%). But the overall trend shows that the error gradually increases with the increase in the time of use, which verifies the effectiveness of the proposed method. That is, the error between the expected and actual returns can be significantly reduced by using the proposed method.

In engineering practice, the capacity configuration of energy storage is mostly based on current data as support, which is not reliable. The method proposed in this article can provide relatively complete data support for ESS capacity configuration only based on limited data. In addition, the method in this article does not involve more complex operations and is easier to generalize. For example, when users consider building small distributed power generation equipment, according to the method in this article, they only

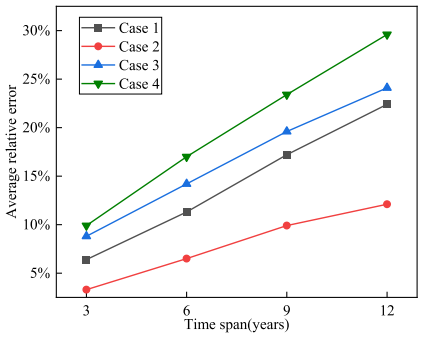

FIGURE 12. Relative error curve for different regions.

need to collate and analyze historical power consumption data to obtain relatively complete conclusions.

V. CONCLUSION AND OUTLOOK

In this paper, we propose a Long-term ESS capacity configuration method based on IGFM. The following conclusions can be drawn from the simulation case:

1) Compared with GFM, the reliability, and accuracy of IGFM prediction have been improved.

2) We propose an ingenious method to solve the obtained economic and social benefits, which not only improves the convergence accuracy and speed but also maximizes the social benefits without damaging the economic benefits.

3) Compared with the commonly used short-term typical data for capacity configuration, we fully consider the economic benefits and social benefits achieved during the whole life cycle of distributed generation and reveal the nonlinear relationship between the benefits, capacity, and service life, which is very valuable and can greatly reduce the error between the actual benefits and the expected benefits.

There are still some deficiencies in this paper. For example, we did not take into account the significant changes in load characteristics due to policy changes, and the scheduling effects that can be achieved when there is greater uncertainty in the load. In the subsequent research, we will take full account of the uncertainty of load, policy changes, and other factors to further enrich ESS capacity configuration methods.

REFERENCES

[1] D. Shindell and C. J. Smith, "Climate and air-quality benefits of a realistic phase-out of fossil fuels," *Nature*, vol. 573, no. 7774, pp. 408–411, Sep. 2019, doi: 10.1038/s41586-019-1554-z.

[2] Y. Cheng, "Low-carbon operation of multiple energy systems based on energy-carbon integrated prices," *IEEE Trans. Smart Grid*, vol. 11, no. 2, pp. 1307–1318, Aug. 2019, doi: 10.1109/TSG.2019.2935736.

[3] R. Dufo-López, I. R. Cristóbal-Monreal, and J. M. Yusta, "Stochastic-heuristic methodology for the optimisation of components and control variables of PV-wind-diesel-battery stand-alone systems," *Renew. Energy*, vol. 99, pp. 919–935, Dec. 2016, doi: 10.1016/j.renene.2016.07.069.

[4] A. La Fata, M. Brignone, R. Procopio, S. Bracco, F. Delfino, R. Barilli, M. Ravasi, and F. Zanellini, "An efficient energy management system for long term planning and real time scheduling of flexible polygeneration systems," *Renew. Energy*, vol. 200, pp. 1180–1201, Nov. 2022, doi: 10.1016/j.renene.2022.10.030.

[5] L. Tziovani, L. Hadjidemetriou, C. Charalampous, M. Tziakouri, S. Timotheou, and E. Kyriakides, "Energy management and control of a flywheel storage system for peak shaving applications," *IEEE Trans. Smart Grid*, vol. 12, no. 5, pp. 4195–4207, Sep. 2021, doi: 10.1109/TSG.2021.3084814.

[6] A. Fathi, Q. Shafiee, and H. Bevrani, "Robust frequency control of microgrids using an extended virtual synchronous generator," *IEEE Trans. Power Syst.*, vol. 33, no. 6, pp. 6289–6297, Nov. 2018, doi: 10.1109/TPWRS.2018.2850880.

[7] E. Tsioumas, N. Jabbour, M. Koseoglou, and C. Mademlis, "A novel control strategy for improving the performance of a nearly zero energy building," *IEEE Trans. Power Electron.*, vol. 35, no. 2, pp. 1513–1524, Feb. 2020, doi: 10.1109/TPEL.2019.2921107.

[8] D. J. Olsen and D. S. Kirschen, "Profitable emissions-reducing energy storage," *IEEE Trans. Power Syst.*, vol. 35, no. 2, pp. 1509–1519, Mar. 2020, doi: 10.1109/TPWRS.2019.2942549.

[9] E. Tsioumas, N. Jabbour, M. Koseoglou, D. Papagiannis, and C. Mademlis, "Enhanced sizing methodology for the renewable energy sources and the battery storage system in a nearly zero energy building," *IEEE Trans. Power Electron.*, vol. 36, no. 9, pp. 10142–10156, Sep. 2021, doi: 10.1109/TPEL.2021.3058395.

[10] Z. Guo, W. Wei, L. Chen, M. Shahidehpour, and S. Mei, "Distribution system operation with renewables and energy storage: A linear programming based multistage robust feasibility approach," *IEEE Trans. Power Syst.*, vol. 37, no. 1, pp. 738–749, Jan. 2022, doi: 10.1109/TPWRS.2021.3095281.

[11] E. Chaerun Nisa and Y.-D. Kuan, "Comparative assessment to predict and forecast water-cooled chiller power consumption using machine learning and deep learning algorithms," *Sustainability*, vol. 13, no. 2, p. 744, Jan. 2021, doi: 10.3390/su13020744.

[12] C. Song, G. Han, and P. Zeng, "Cloud computing based demand response management using deep reinforcement learning," *IEEE Trans. Cloud Comput.*, vol. 10, no. 1, pp. 72–81, Jan. 2022, doi: 10.1109/TCC.2021.3117604.

[13] Z. A. Shah, H. F. Sindi, A. Ul-Haq, and M. A. Ali, "Fuzzy logic-based direct load control scheme for air conditioning load to reduce energy consumption," *IEEE Access*, vol. 8, pp. 117413–117427, 2020, doi: 10.1109/ACCESS.2020.3005054.

[14] M. Jalali and O. Alizadeh-Mousavi, "Application of real-time distribution grid monitoring for grid forecasting and control considering incomplete information of resources behind-the-meter," *IEEE Open Access J. Power Energy*, vol. 9, pp. 308–318, 2022, doi: 10.1109/OAJPE.2022.3195755.

[15] K. Antoniadou-Plytaria, D. Steen, L. A. Tuan, O. Carlson, and M. A. F. Ghazvini, "Market-based energy management model of a building microgrid considering battery degradation," *IEEE Trans. Smart Grid*, vol. 12, no. 2, pp. 1794–1804, Mar. 2021, doi: 10.1109/TSG.2020.3037120.

[16] H. Jiang, E. Du, and C. Jin, "Optimal planning of multi-time scale energy storage capacity of cross-national interconnected power system with high proportion of clean energy," *Proc. CSEE*, vol. 41, no. 6, pp. 2101–2115, Jan. 2021.

[17] P. Roy, J. He, and Y. Liao, "Cost minimization of battery-supercapacitor hybrid energy storage for hourly dispatching wind-solar hybrid power system," *IEEE Access*, vol. 8, pp. 210099–210115, 2020, doi: 10.1109/ACCESS.2020.3037149.

[18] M. Cucuzzella, T. Bouman, K. C. Kosaraju, G. Schuitema, N. H. Lemmen, S. Johnson-Zawadzki, C. Fischione, L. Steg, and J. M. A. Scherpen, "Distributed control of DC grids: Integrating prosumers' motives," *IEEE Trans. Power Syst.*, vol. 37, no. 4, pp. 3299–3310, Jul. 2022, doi: 10.1109/TPWRS.2021.3109024.

[19] C. Leone, M. Longo, L. M. Fernandez-Ramirez, and P. Garcia-Trivino, "Multi-objective optimization of PV and energy storage systems for ultra-fast charging stations," *IEEE Access*, vol. 10, pp. 14208–14224, 2022, doi: 10.1109/ACCESS.2022.3147672.

[20] B. Zhang, P. Dehghanian, and M. Kezunovic, "Optimal allocation of PV generation and battery storage for enhanced resilience," *IEEE Trans. Smart Grid*, vol. 10, no. 1, pp. 535–545, Jan. 2019, doi: 10.1109/TSG.2017.2747136.

[21] B. Celik, R. Roche, D. Bouquain, and A. Miraoui, "Decentralized neighborhood energy management with coordinated smart home energy sharing," *IEEE Trans. Smart Grid*, vol. 9, no. 6, pp. 6387–6397, Nov. 2018, doi: 10.1109/TSG.2017.2710358.

[22] S. A. Mansouri, A. Ahmarinejad, E. Nematbakhsh, M. S. Javadi, A. R. Jordehi, and J. P. S. Catalão, "Energy management in microgrids including smart homes: A multi-objective approach," *Sustain. Cities Soc.*, vol. 69, Jun. 2021, Art. no. 102852, doi: 10.1016/j.scs.2021.102852.

[23] K. Thirugnanam, M. S. E. Moursi, V. Khadkikar, H. H. Zeineldin, and M. A. Hosani, "Energy management strategy of a reconfigurable grid-tied hybrid AC/DC microgrid for commercial building applications," *IEEE Trans. Smart Grid*, vol. 13, no. 3, pp. 1720–1738, May 2022.
[24] M. Tofighi-Milani, S. Fattaheian-Dehkordi, M. Fotuhi-Firuzabad, and M. Lehtonen, "Decentralized active power management in multi-agent distribution systems considering congestion issue," *IEEE Trans. Smart Grid*, vol. 13, no. 5, pp. 3582–3593, Sep. 2022, doi: 10.1109/TSG.2022.3172757.
[25] Y. Tao, J. Qiu, S. Lai, and J. Zhao, "Integrated electricity and hydrogen energy sharing in coupled energy systems," *IEEE Trans. Smart Grid*, vol. 12, no. 2, pp. 1149–1162, Mar. 2021, doi: 10.1109/TSG.2020.3023716.
[26] P. Zhao, C. Gu, F. Li, and X. Yang, "Battery storage configuration for multi-energy microgrid considering primary frequency regulation and demand response," *Energy Rep.*, vol. 8, pp. 1175–1183, Nov. 2022, doi: 10.1016/j.egyr.2022.06.086.
[27] T. T. Nguyen, T. T. Nguyen, and B. Le, "Artificial ecosystem optimization for optimizing of position and operational power of battery energy storage system on the distribution network considering distributed generations," *Expert Syst. Appl.*, vol. 208, Dec. 2022, Art. no. 118127, doi: 10.1016/j.eswa.2022.118127.
[28] P. Xie, Y. Jia, C. Lyu, H. Wang, M. Shi, and H. Chen, "Optimal sizing of renewables and battery systems for hybrid AC/DC microgrids based on variability management," *Appl. Energy*, vol. 321, Sep. 2022, Art. no. 119250, DOI10.1016/j.apenergy.2022.119250.
[29] Z. Yang, J. Hu, X. Ai, J. Wu, and G. Yang, "Transactive energy supported economic operation for multi-energy complementary microgrids," *IEEE Trans. Smart Grid*, vol. 12, no. 1, pp. 4–17, Jan. 2021, doi: 10.1109/TSG.2020.3009670.
[30] Y. Zhou, Q. Zhai, and L. Wu, "Optimal operation of regional microgrids with renewable and energy storage: Solution robustness and nonanticipativity against uncertainties," *IEEE Trans. Smart Grid*, vol. 13, no. 6, pp. 4218–4230, Nov. 2022, doi: 10.1109/TSG.2022.3185231.
[31] A. M. Abdelshafy, J. Jurasz, H. Hassan, and A. M. Mohamed, "Optimized energy management strategy for grid connected double storage (pumped storage-battery) system powered by renewable energy resources," *Energy*, vol. 192, Feb. 2020, Art. no. 116615, doi: 10.1016/j.energy.2019.116615.
[32] H. Lu, M. Zhang, Z. Fei, and K. Mao, "Multi-objective energy consumption scheduling in smart grid based on Tchebycheff decomposition," *IEEE Trans. Smart Grid*, vol. 6, no. 6, pp. 2869–2883, Nov. 2015, doi: 10.1109/TSG.2015.2419814.
[33] X. Liang, X. He, and T. Huang, "Distributed neuro-dynamic optimization for multi-objective power management problem in micro-grid," *Neurocomputing*, vol. 362, pp. 51–59, Oct. 2019, doi: 10.1016/j.neucom.2019.05.096.
[34] U. T. Salman, F. S. Al-Ismail, and M. Khalid, "Optimal sizing of battery energy storage for grid-connected and isolated wind-penetrated microgrid," *IEEE Access*, vol. 8, pp. 91129–91138, 2020, doi: 10.1109/ACCESS.2020.2992654.
[35] J. L. Deng, *Grey Control System*. Wuhan, China: Huazhong Univ. Sci. Technol. Press, 1995.
[36] N. Xie, "Explanations about grey information and framework of grey system modeling," *Grey Syst., Theory Appl.*, vol. 7, no. 2, pp. 179–193, Aug. 2017, doi: 10.1108/GS-05-2017-0012.
[37] W. Zhang, Q. Chen, J. Yan, S. Zhang, and J. Xu, "A novel asynchronous deep reinforcement learning model with adaptive early forecasting method and reward incentive mechanism for short-term load forecasting," *Energy*, vol. 236, Dec. 2021, Art. no. 121492, doi: 10.1016/j.energy.2021.121492.
[38] M. Tan, S. Yuan, S. Li, Y. Su, H. Li, and F. H. He, "Ultra-short-term industrial power demand forecasting using LSTM based hybrid ensemble learning," *IEEE Trans. Power Syst.*, vol. 35, no. 4, pp. 2937–2948, Jul. 2020, doi: 10.1109/TPWRS.2019.2963109.
[39] C. Kuster, Y. Rezgui, and M. Mourshed, "Electrical load forecasting models: A critical systematic review," *Sustain. Cities Soc.*, vol. 35, pp. 257–270, Nov. 2017, doi: 10.1016/j.scs.2017.08.009.

JIFANG LI was born in Kaifeng, Henan, China, in 1971. He received the M.S. degree in control technology from the Huazhong University of Science and Technology, Wuhan, in 2003, and the Ph.D. degree in power electronics and power transmission from Shanghai Maritime University, Shanghai, in 2011. He is currently a Professor with the College of Electricity, North China University of Water Resources and Electric Power. His current research interests include grid dispatching and the fault diagnosis of smart grids.

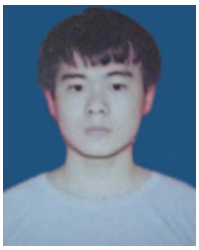

SHUO FENG was born in Shangqiu, Henan, China, in 1995. He is currently pursuing the master's degree with the North China University of Water Resources and Electric Power. His current research interest includes power system scheduling and planning.

TAO ZHANG was born in Luoyang, Henan, China, in 1977. He is currently with State Grid Henan Electric Power Company Luoyang Power Supply Company. His current research interest includes the fault diagnosis of smart grids.

LIDONG MA was born in Zhoukou, Henan, China, in 1995. He is currently pursuing the master's degree with the North China University of Water Resources and Electric Power. His current research interest includes substation status estimation.

XIAOYANG SHI was born in Luoyang, Henan, China, in 1999. He is currently pursuing the master's degree with the North China University of Water Resources and Electric Power. His current research interests include online monitoring and the fault diagnosis of smart grids.

XINGYAO ZHOU was born in Zhengzhou, Henan, China, in 1997. He is currently pursuing the master's degree with the North China University of Water Resources and Electric Power. His current research interest includes integrated energy systems.